IAC-13.C1.8.4

MANOEUVRING CONSIDERATIONS FOR QUASI-PERIODIC TRAJECTORIES

Marcel Duering
University of Strathclyde, Advanced Space Concepts Laboratory
email: marcel.duering@strath.ac.uk

Massimiliano Vasile
University of Strathclyde, Advanced Space Concepts Laboratory
email: massimiliano.vasile@strath.ac.uk

Markus Landgraf
Mission Analysis Section, ESA/European Space Operations Centre
email: markus.landgraf@esa.int

Abstract The lunar vicinity attracts attention in particular for long-duration human exploration enabling complex missions to multiple destinations. A variety of orbits exist near the Lagrangian points L_1 and L_2 that can serve as nominal orbit for such mission scenarios. One type so-called quasi-periodic orbits are studied in this paper for this purpose. Those orbits are associated with frequencies, phases, and amplitudes. The existence and main characteristics of quasi-periodic orbits around the far-side Lagrangian point in the Earth-Moon system are studied. Stability directions and corresponding stable and unstable manifold branches are determined and compared. A parametric set in angular phase space is introduced for the orbits and their hyperbolic invariant manifolds. Solutions are identified to transfer spacecraft between quasi-periodic orbits and to compensate phase differences between spacecraft bringing together the parametric orbit and manifold representation. The proposed technique utilise the stable manifold allowing for single manoeuvre transfers. The transfers are classified and characterised. Two transfer scenarios within the orbit families are discussed with respect to future missions that have to cope with regular vehicle traffic, rendezvous and docking activities. In the first case, two spacecraft are separated from a halo orbit and distributed on a quasi-periodic orbit. In the second case, a given phase difference between two spacecraft is compensated and a target orbit is defined in which the spacecraft finally rendezvous. Parameter studies show the existence of those transfers and their strong dependence on the time when the manoeuvre is performed.

I INTRODUCTION

The lunar vicinity describes the space around the Moon enclosed by the two co-linear Lagrangian points. The dynamics in this region is modelled as a three-body problem (CRTBP). The Lagrangian points are equilibrium points named ($L_1 - L_5$), which are also called libration points. L_1 and L_2 are located along the Earth-Moon line with a distance of about 60000 km to the centre of the Moon. Periodic orbits defined in the rotating frame exist around each libration point. There are families of halo orbits symmetric about the $\{xz\}$-plane, vertical lyapunov orbits symmetric about the $\{xy\}$-plane, and planar horizontal lyapunov orbits. Around those periodic orbits are a variety of quasi-periodic orbits. They have the particularity that during its dynamical evolution the trajectories remain on a toroidal surface surrounding the generating orbit. This surface is described as invariant tori in a dynamic system perspective. An example of a quasi-periodic orbit is shown in Fig. 1b. The lunar vicinity is of interest in particular for long-duration human exploration enabling complex missions to multiple destinations. Concepts are required for crew and cargo access and storing beyond Earth orbit in conjunction with payloads delivery. Some infrastructure at L_2 could provide access to the lunar surface and serve as a fuel storage and transportation system for interplanetary missions [2]. The above described (quasi-)periodic trajectories can serve as nominal orbit for such an infrastructure. The Lagrangian point regions are particularly suitable for missions that rely on regular manoeuvres, as a high Δv is required for the transfer, but once arrived all other Δv requirements are relatively small. Manoeuvring spacecraft between different orbits become a key element for such missions in order to cope with regular in-space operations, rendezvous, docking ac-

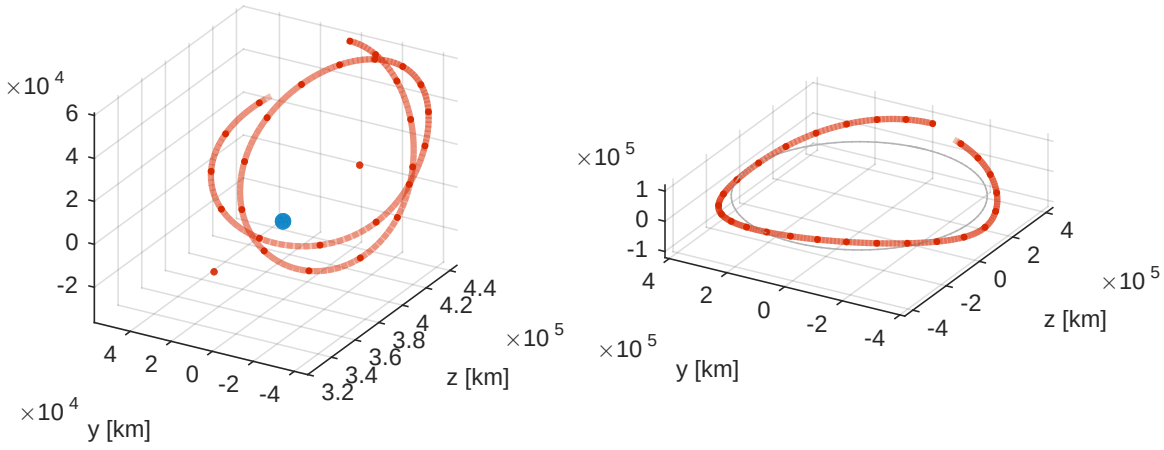

(a) (b)

Figure 1: (a) Trajectory in the rotating reference frame, (b) in the inertial reference frame. Ticks along trajectory represent equal time steps. Trajectory of the Moon plotted in light gray.

tivities. The utilisation of quasi-periodic orbits increases the flexibility in planning the missions. The complexity of long-term space missions would decrease, if e.g. any time access is a driving requirement and a variety of phasing opportunities are available. For example, new launch opportunities arise if multiple phasing options exist, or if multiple spacecraft will be launched on the same rocket and then separated in the proximity of the Lagrangian point. Apart from such a separation scenario, transfers to nearby orbits become relevant for a gateway station concept where locations for e.g. storage are investigated. The naturally existing trajectories in the proximity of a nominal orbit provide optional operation orbits and enable an increased operational flexibility in terms of launch windows and rendezvous scenarios. In this paper, transfers between orbits are studied with respect to those scenarios.

Section II gives insight into the calculation and existence of quasi-periodic orbits and their range in frequencies and amplitudes around the far-side Lagrange point in the Earth-Moon system. It is followed by the description of the stability directions and their stable and unstable manifolds in Section III. For both the orbit and their manifold parametric sets are introduced. In Section IV, the methodology is described to determine optimal manoeuvres to adapt phase and frequency properties of a quasi-periodic orbit. In Section VI, the procedure is applied to identify transfers between quasi-periodic orbits. Two transfer scenarios within the orbit families are discussed. In the first case, two spacecraft are separated from a halo orbit and distributed on a quasi-periodic orbit. In the second case, a given phase difference between two spacecraft is compensated.

II PARAMETRIC REPRESENTATION OF QUASI-PERIODIC ORBITS

For the transfer design it is important to have a parametric description of quasi-periodic trajectories and their associated manifolds, see Section IV. The parametric representation of quasi-periodic orbits enable the identification of a single orbit by the Jacobian constant C and two frequencies ω_1 and ω_2. Furthermore, utilising the parametric representation the location of a spacecraft on the orbit is uniquely defined by two phase angles α and β. The angles are similar to the true anomaly known from the keplerian motion. The computation of quasi-periodic orbits is based on an iterative mapping scheme utilising a Fourier representation to describe an invariant curve representing the intersection of the orbit on a Poincaré section plane. The basic algorithm is described in detail in literature [3, 4, 5], and is modified to additionally provide the parametric representation and system frequencies. A detailed description of invariant tori and their existence is found literature [6].

II.I General mapping process

The mapping process is as followed: The two frequencies are defined as

$$\omega = \{\omega_1, \omega_2\} \tag{1}$$

The first frequency is associated with the orbital period of the generating periodic orbit and describes the motion along this direction. The second frequencies indicates the rotational motion about

the generating periodic orbit. The corresponding angular phase definitions are

$$\begin{aligned} \alpha_i &= \frac{2\pi}{N_1} \qquad i = 0, 1, ..., (N_1 - 1) \\ \beta_j &= \frac{2\pi}{N_2} \qquad j = 0, 1, ..., (N_2 - 1) \end{aligned} \tag{2}$$

The process starts with a definition of the six dimensional state vector along a closed invariant curve.

$$\mathbf{X} = \frac{C_1}{\sqrt{2}} + \sum_{n=1}^{n_{max}} (C_{2n-1} cos(n\beta_n) + C_{2n} sin(n\beta_n)) \tag{3}$$

The transformation from X into Fourier coefficients is defined by matrix W.

$$X = W(\beta) \cdot C \tag{4}$$

where C is the vector containing the Fourier coefficients a_k and b_k. The projection variables are defined as

$$\begin{aligned} X^{projection} &= \Phi_{2\pi/\omega_1}(X_{section}) \\ \beta^{projection} &= \beta^{section} + \omega_2 2\pi/\omega_1 \end{aligned} \tag{5}$$

The error is evaluated as

$$E = X^{projection} - W(\beta^{projection}) \cdot C \tag{6}$$

At the beginning of the process both frequencies are unknown. An initial guess for the frequencies is obtained from properties of the generating periodic orbit. The objective is to find the closed curve $X_{section}$ and the two frequencies such that the error function is zero, $E = 0$. The Newton update is defined as

$$Q_{i+1} = Q_i - \frac{DF(Q_i)}{F(Q_i)} \tag{7}$$

where

$$\begin{aligned} Q &= \{C, \omega_1, \omega_2\} \\ F &= \{E, en, ze, ae\} \end{aligned} \tag{8}$$

Three constraints are required to uniquely define the orbit. Two constraints define a member within the family of possible solutions. One energy constraint and the other assuring the family continuation by restricting the x component of the parametric point $(0, 0)$. The third constraint fixes the orientation of the phase definition as this is arbitrary defined. Once the system is solved the parametric function u is extended to the entire invariant torus. The solution can be interpreted as a parametric solution for $u(0, \beta^s)$, and the unknown values for u are obtained by integration:

$$u_{i,j} = \Phi_{2\pi/\omega_1 \alpha_i}(X^{section}(\beta_j)) \tag{9}$$

Further interpolation is required for equally spaced results on the domain of β at that point.

II.II Families of quasi-periodic orbits

By applying the previously introduced method to a wide range of periodic orbits around L_2, families of quasi-periodic orbits are computed. The four-dimensional centre manifold around L_2 is occupied by quasi-periodic orbits of two different families, the Lissajous family around vertical Lyapunov orbits (type II), and the ones around halo orbits (type I), see Figure 3. The two system frequencies show a different trend within the family. For type I, ω_1 decreases with the family continuation, while ω_2 increases. For type II, both frequencies increase. The Jacobian constant and therefore the energy is equal for all trajectories in Figure 3. A Poincaré map for $z = 0$ and a Jacobian constant $C = 3.0292$ is shown in Figure 2. The periodic orbits are reduced to points, the halo orbit appears as pair dots symmetric to the $\{xz\}$-plane, the vertical lyapunov as single green dot. The position of the Moon (red) and the Lagrangian point L_2 (black) appear on the $\{y\}$-axis. The horizontal lyapunov orbit restrict the families of quasi-periodic orbits (outer black line). The Jacobian constant and the two frequencies uniquely describe an orbit of the quasi-periodic family. The solution space for both types of orbits is shown in Figure 4. The existence is restricted to right by the orbital period of the generating periodic orbit and the corresponding ω_2 as the argument of the complex eigenvalue of the monodromy matrix. The maximal extend is given

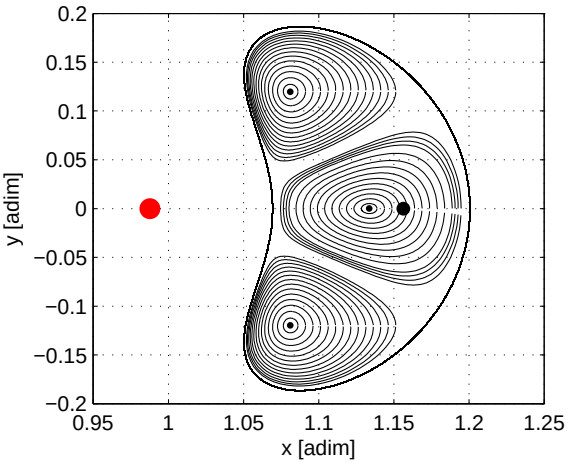

Figure 2: Poincaré map $z = 0$ for a Jacobian constant of $C = 3.0292$.

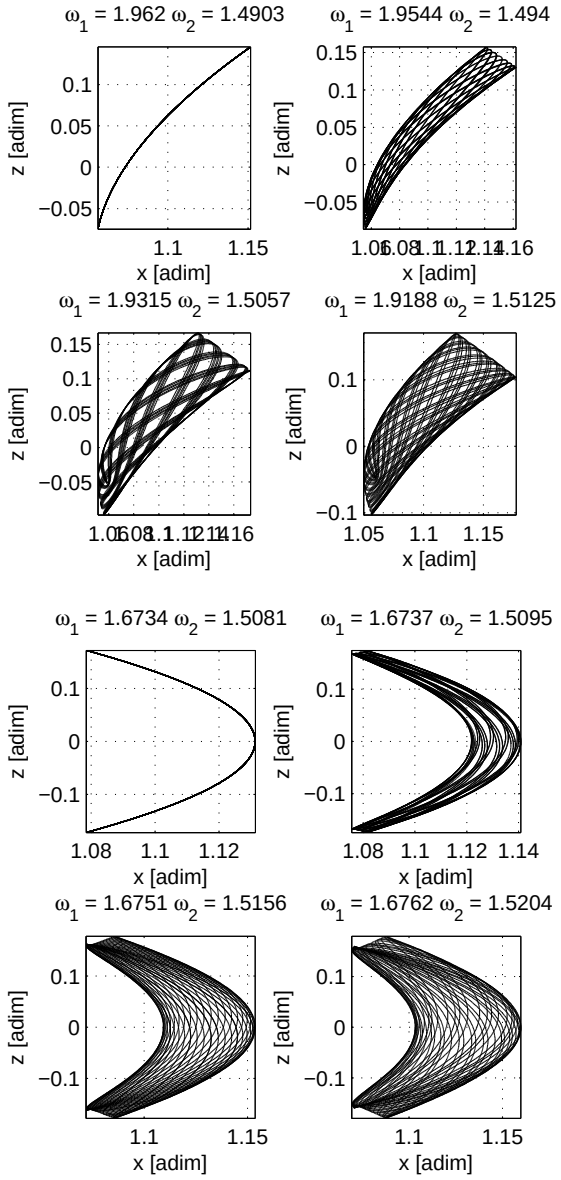

Figure 3: Quasi-periodic orbits around a northern halo orbit (type I) (top), and around a vertical lyapunov orbit (type II) (bottom).

by the same pair of frequencies of the horizontal lyapunov orbits.

III STABILITY OF QUASI-PERIODIC ORBITS

The stability information required for the next Section are the stable and unstable directions. The general stable or unstable behaviour of an orbit is not investigated here. The analysis performed here focus on the required stability information for a periodic orbit that is derived from the normal behaviour, therefore from the eigenvector of the monodromy matrix.

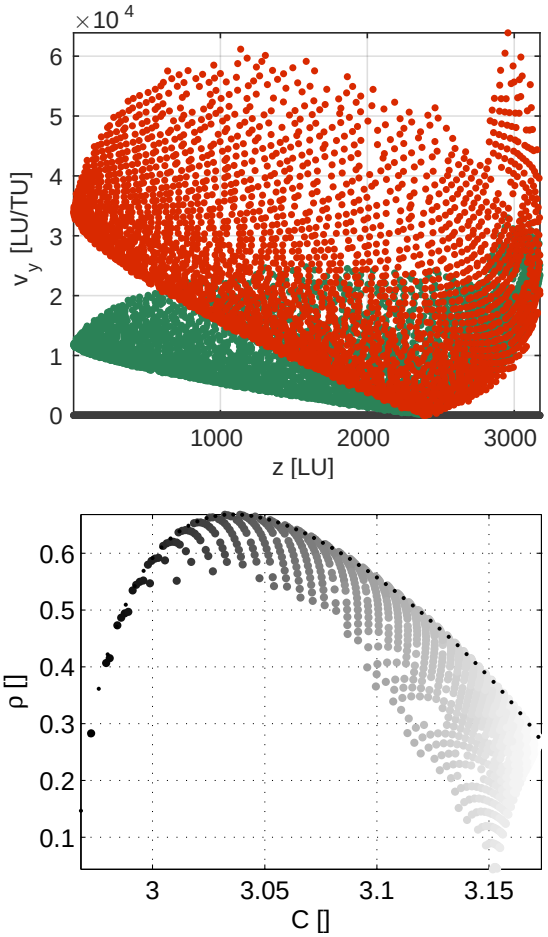

Figure 4: Frequency range within the family of quasi-periodic orbits. Type I (top), type II (bottom).

$$\phi = \Phi_{2\pi/\omega_1}(u) \tag{10}$$

The eigenvalues and corresponding eigenvectors define the stability of the orbit. The real eigenvalues λ (> 1) the unstable, and λ^{-1} (< 1) the stable direction. For a periodic orbit the definition is

$$\begin{aligned} \psi^u &= \lambda^{\alpha/2\pi}\Phi_{2\pi/\omega_1\alpha}(u) \\ \psi^s &= \lambda^{-\alpha/2\pi}\Phi_{2\pi/\omega_1\alpha}(u) \end{aligned} \tag{11}$$

For the quasi-periodic orbit an intermediate step is required to cancel the rotation caused by the dynamic of the invariant torus. The stability calculation is partially a by-product of the previous described iterative calculation of the torus parametrisation. Again, the definition of the state transition matrix is

$$\phi_{i,j} = \Phi_{2\pi/\omega_1}(u_{i,j}) \tag{12}$$

Rotation operator

$$R(-\rho) = D^{-1}Q(-\rho)D \tag{13}$$

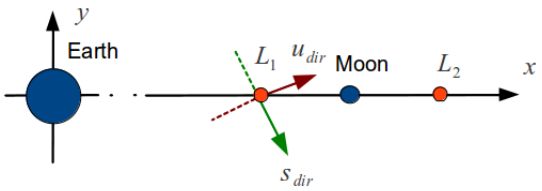

Figure 5: Definition of the stable and unstable directions around L_1.

Block diagonal matrix F_x

$$F_x = diag\,(\phi_{0,0}, \phi_{0,1}, ..., \phi_{0,N}) \tag{14}$$

$$M = R(-\rho)F_x \tag{15}$$

The eigenvalues and eigenvectors of M contain the required stability information. Once the stability directions are determined for the first closed curve, the set is complemented by integration with the following definitions

$$\begin{aligned} \psi^u_{i,j} &= \lambda^{-\alpha_i/2\pi}\Phi_{2\pi/\omega_1\alpha_i}(u_{i,j}) \\ \psi^s_{i,j} &= \lambda^{\alpha_i/2\pi}\Phi_{2\pi/\omega_1\alpha_i}(u_{i,j}) \end{aligned} \tag{16}$$

III.I Stability directions

The stability directions are defined by the angle between the velocity component of the eigenvectors and the $\{x\}$-axis of the rotating coordinate frame $(1, 0, 0)$. In theory derived from the linear lissajous motion the angle between the stable and unstable direction is 90 deg, whereas the stable direction angle is -65.31 deg and the unstable one 24.69 deg [1]. In this case the angle is only defined in the $\{xy\}$-plane with no component in $\{z\}$-direction. The defined angle is shown in Figure 6 (top) for a periodic orbit within in the vertical lyapunov family ($C = 3.0283$) over one orbital period. The angle for both direction oscillate around the constant value known from the linear lissajous motion. For a better comparison, the angle is once evaluated for a pure in-plane case (light colours) and for the spatial direction (bright colours).

A similar behaviour occurs for the stability directions a quasi-periodic orbit. The results are similar to the periodic case, as seen in Figure 6 (bottom). Major difference is that instead of a single stability direction angle the entire range of β the stability angles are plotted. The information gained is not only important for the calculation of the stable and unstable manifold directions, but for e.g. thruster alignment during early spacecraft mission design.

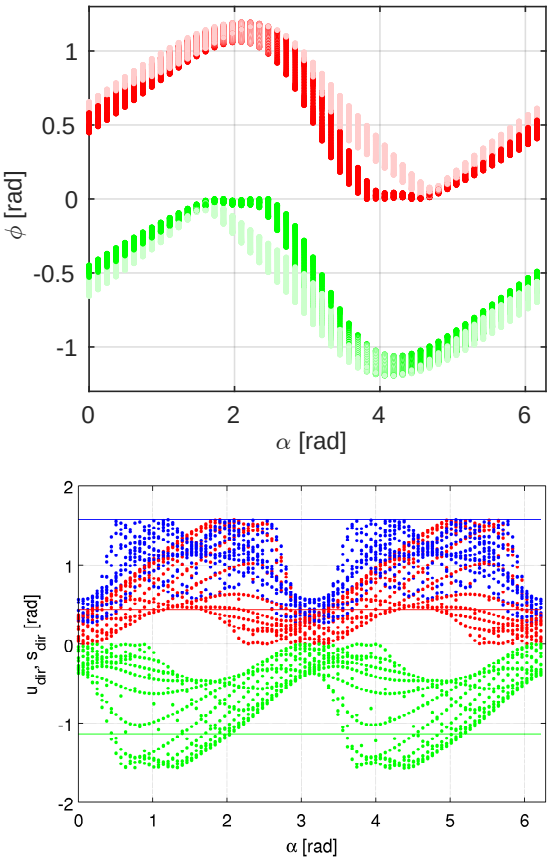

Figure 6: Stable (green) and unstable (red) direction angles for a periodic orbit (top) and for a quasi-periodic orbit (bottom).

III.II (Un)stable invariant manifolds

The stable (unstable) manifold is created by perturbing a state on the quasi-periodic orbit in the stable (unstable) direction defined in the previous Section, and followed by backward (forward) propagation. This manoeuvre forces the spacecraft to move towards the (un)stable invariant manifold. Both, stable and unstable invariant manifolds have a positive and a negative branch. One approaches the Moon, whereas the other one leaves the Lagrangian point region to the opposite direction. In this study only the manifold structure in the proximity of the orbit is relevant as the connections between different orbits and not transfers to the primary or secondary body are studied, see Section IV. The visualisation o the (un)stable invariant manifolds is very difficult as they are high dimensional structures in space. Snapshots at three different times are shown in Figure 7.

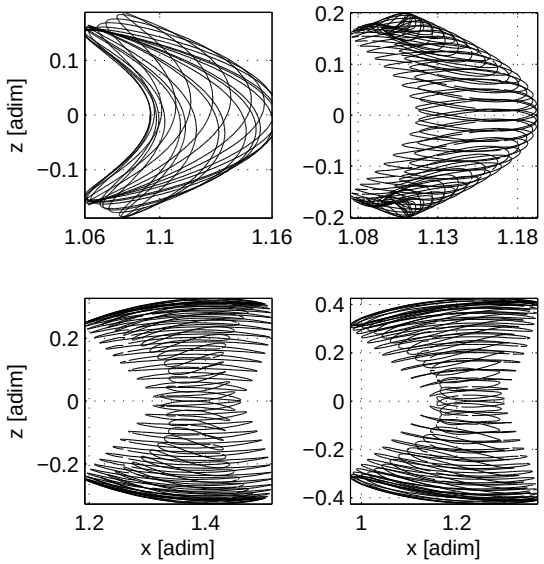

Figure 7: Quasi-periodic trajectory (top,left). Manifold snapshots from negative branch $t = -3.0$ (top, right), $t = -5.0$ (bottom, left), $t = -6.0$ (bottom, right).

IV TRANSFERS WITHIN THE FAMILY OF QP-ORBITS

In this section feasible transfers are studied from one orbit to another within the family of periodic and quasi-periodic orbits. Depending on the case a transfer can change the properties of the trajectory or the location of the spacecraft along its path. The following cases are studied:

- Transfers from periodic orbit $x(\omega_1, C)$ to qp-orbit $x(\omega_1, \omega_2, C)$, this results in changing (ω_1, ω_2, C) and the phases (α, β) by the manoeuvre.
- Transfers from qp-orbit $x(\omega_1, \omega_2, C)$ to qp-orbit $x(\omega_1, \omega_2, C)$, this results in maintaining (ω_1, ω_2, C) but changing the phases (α, β) by the manoeuvre.
- Transfers from qp-orbit $x(\omega_1^1, \omega_2^1, C^1)$ to qp-orbit $x(\omega_1^2, \omega_2^2, C^2)$, the transfer changes the entire set of parameters.

Other scenarios are possible but not studied in this paper. The application reaches from finding heteroclinic and homoclinic connections to the design of transfer arcs from the primary and secondary body to the orbit that is investigated. The focus is set on transfers that utilise the manifold structure of the quasi-periodic orbit. The idea is to construct transfers by matching the outgoing manifold branch with the final orbit. The result is that a manoeuvre is conducted at time t, and after the velocity change the spacecraft continues its path along a stable manifold leading to the final orbit. This method offers lower Δv expenses for the transfer compared to two-impulse transfer arcs. The methodology brings together the parametric representation of the orbit and manifold. The methodology is described in the following section.

IV.I Identification of feasible transfer sets

The transfer path construction process starts with the determination of feasible parameter combinations. The initial and target locations of the spacecraft on a quasi-periodic trajectory are represented by four angular coordinates α^i, β^i, α^f and β^f. Instead of using numerical propagation, all parameter combinations are scanned by using the analytic function u, and evaluating the distance and Δv requirements. The parameter sets are determined by introducing discrete steps for each parameter. The identification of feasible transfer parameter sets is realised by a differential evolution algorithm. This leaves two optimisation parameters, which are Δv_x and Δv_y. Alternatively the direction θ and magnitude $|\Delta v|$ can be defined. A differential evolution (DE) algorithm for non-linear functions is used to drive the norm of the manoeuvre to a minimum. The size of the population is set to $N = 20$ and 200 generations are calculated. The differential evolution algorithm has two parameter subject to adaptation, the differential weight $F = [0, 2]$ and $CR = [0, 1]$ representing the crossover probability. The tuning parameters CR and F are set to $[0.5, 0.8]$ for our purpose.

Optimisation parameter

- phase angles on initial orbit α_i and β_i
- α_f and β_f for the targeted orbit
- transfer time along hyperbolic invariant manifold branch t_f
- hyperbolic invariant manifold branch i $[-11]$

Cost function and constraint handling

1. Maximizing the orbital lifetime $J = max(T_m^+)$ downstream
2. Δv chosen to maximize the mean lifetime $J = mean(T_m^+, T_m^-)$ both upstream and downstream. This only leads to feasible solutions if the velocity vector is accurate.
3. A multi-objective optimisation with the cost functions $J_1 = max(T_m^+)$ and $J_2 = min(\Delta v)$

The location of the spacecraft at arrival and departure are evaluated with the help of the parametric function u. This enable the use of α and β as optimisation variables without numerical integration of the final trajectory. The following cost function is used to calculate possible regions of the five-dimensional solution space

$$f = \begin{cases} u\left(\alpha^i, \beta^i\right) - \Phi_{-\tau}\left(u\left(\alpha^i, \beta^i\right) + \epsilon\psi\left(\alpha^i, \beta^i\right)\right) \\ u\left(\alpha^i, \beta^i\right) - \Phi_{-\tau}\left(u\left(\alpha^i, \beta^i\right) + \epsilon\psi\left(\alpha^i, \beta^i\right)\right) \end{cases} \tag{17}$$

The cost function for the case with two transfer arcs one on the stable and the other one on the unstable manifold branch is defined as

$$f = \begin{cases} u\left(\alpha^i, \beta^i\right) - \Phi_{-\tau}\left(u\left(\alpha^i, \beta^i\right) + \epsilon\psi\left(\alpha^i, \beta^i\right)\right) \\ u\left(\alpha^i, \beta^i\right) - \Phi_{-\tau}\left(u\left(\alpha^i, \beta^i\right) + \epsilon\psi\left(\alpha^i, \beta^i\right)\right) \end{cases} \tag{18}$$

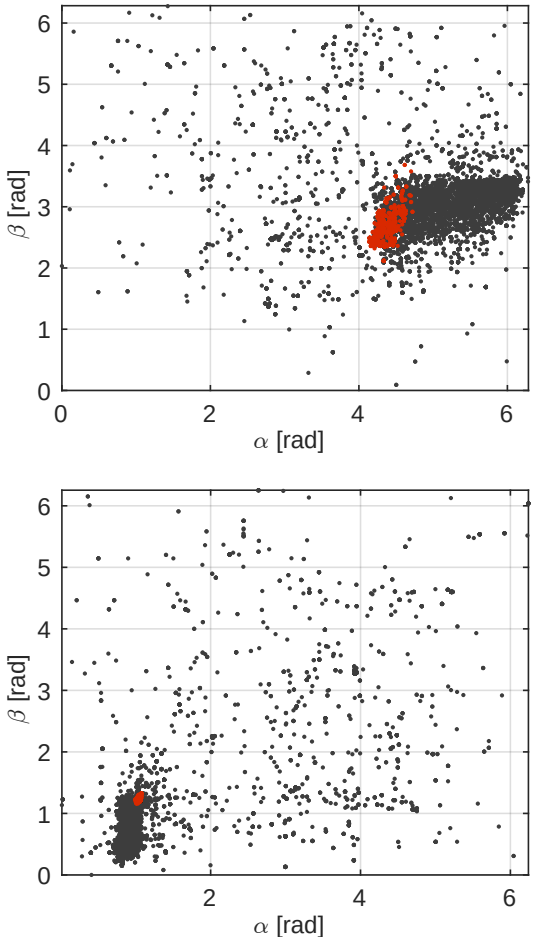

Figure 8: Results of initialisation with initial and final orbit *(left)*. Scanned feasible transfers with position and velocity offset *(right)*.

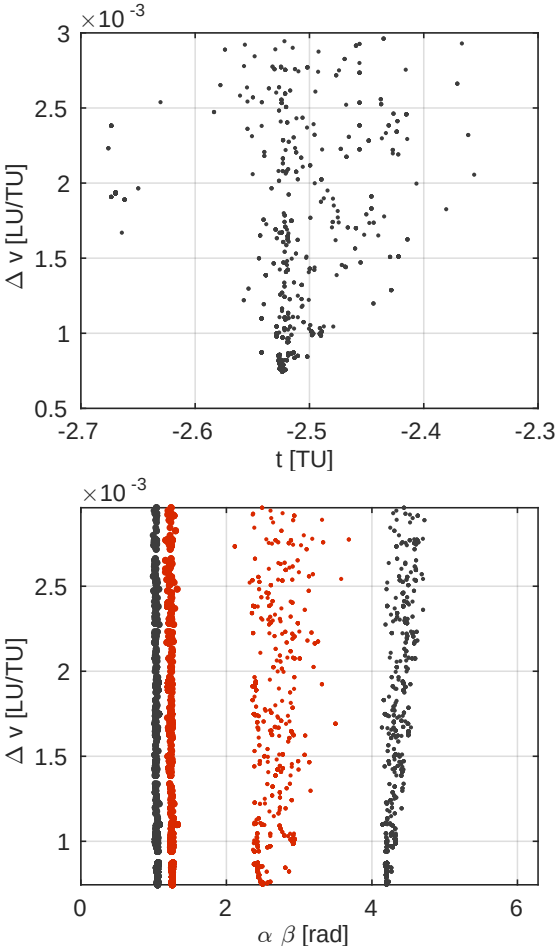

Figure 9: Results of initialisation with initial and final orbit *(left)*. Scanned feasible transfers with position and velocity offset *(right)*.

The entire set of feasible transfers $(\alpha, \beta, t_{tf}, \Delta v_1)$ corresponding to the smallest distance between $x_{qp}(\alpha, \beta)$ and x_0 is evaluated. This is done for states along the initial orbit. The results of a scan is shown in Figure **??** for a scenario of the first case. The qp-orbit of interest is define by $\{1.6744, 1.5465, 3.0704\}$. The plot includes transfer options for both stable manifold branches, the light colors correspond to the positive one, and bright colors to the negative one. The next step is to separate the feasible transfer options, refine and classify them. Selected transfer options over time t along the initial orbit are shown in Figure **??**. The colour of the data points is related to the time when the manoeuvre is executed. A set of phases $\{\alpha, \beta\}$ corresponding to time t is defined as

$$\{\alpha, \beta\} = \{t_i\omega_1, t_i\omega_2\} \qquad \text{mod } 2\pi \tag{19}$$

The Δv and transfer times for all four sets complement the information required additional to the

br.	$t_{transfer}$	α	β	α_{res}	β_{res}
+1	- 2.767	0.314	0.837	6.257	1.004
-1	- 3.514	3.665	1.623	2.469	0.998

Table 1: Notion of the types of quasi-periodic orbit families. Summary of the maximal extend of the bounding boxes for the two-parameter continuation process.

phase tuples, they are shown with respect to time in Figure **??**.

IV.II Transfer optimisation

Once a feasible transfer set is identified, a gradient based optimisation finally creating the transfer arc. In the following the formulation of the transfer problem will be given. The problem is formulated as a matching of a forward and a backward propagated arc with the initial and final phases generated by the guess generation, see previous section. The manoeuvre indirectly defined as the velocity offset at the end of both transfer arcs. For the gradient-based optimisation, the cost function is the magnitude of the first manoeuvre to set the spacecraft onto the transfer trajectory. The optimisation problem can be stated as follows: given an initial and final orbit, determine departing and phasing location on the orbits that a stable manifold branch of the final orbit connects these orbits such that the optimality criterion is fulfilled.

The following list summarises the xxx parameters that are required in the optimisation

- phase angles on initial orbit α_i and β_i
- α_f and β_f for the targeted orbit
- transfer time along hyperbolic invariant manifold branch t_f
- hyperbolic invariant manifold branch i $[-11]$

Cost function and constraint handling

- definition of the feasibility region
- within feasibility region cost evaluation by Δv

Figure **??** depicts the results of the optimisation and the estimates after the filtering for the sample case. It can be observed that the filter provides in general a good approximation of the total cost to be expected. The outcome of the optimisation are locally optimal transfers, with associated arrival and departure conditions, the transfer time, and Δv expenses. The phase shift between the initial and final orbit can be calculated as follows

$$\{\Delta\alpha, \Delta\beta\} = \left\{\alpha^f + \tau\omega^f - \alpha^i, \beta^f + \tau\omega_2^f - \beta^i\right\} \mod 2\pi \tag{20}$$

V TWO TRANSFER SCENARIOS

Two transfer scenarios are investigated. For both scenarios the following two orbits are selected: A periodic orbit from the halo family with $C = 3.1259$, and a quasi-periodic orbit with $\omega_1 = 1.776, \omega_2 = 1.7098, C = 3.1259$. Both trajectories are plotted in Figure 10 from $x = \{0, 6\}$.

V.I Distribution of spacecraft

In the first case, the distribution of spacecraft from a halo orbit onto a quasi-periodic is studied. The use of a single rocket to launch a set of satellites requires such transfers. An efficient way has to be found to separate the satellites either during transfer or once they are inserted into orbit around the Lagrangian point. A single launch with a later deployment enable an increased operational flexibility in terms of launch windows and phasing requirements. Apart from such a separation scenario, transfers to nearby orbits become relevant e.g. for formation deployment. Those transfers are design in the same way as in this scenario. The scenario assumes two spacecraft launched and injected into a halo orbit with a orbital period of $T = 3.36$ dimensionless units (14.59 days). The objective is to distribute them on a quasi-periodic orbit in such a way that the phase difference in the ω_2-direction is 210 deg. In order to find the optimal time for the two transfer manoeuvres, the optimal

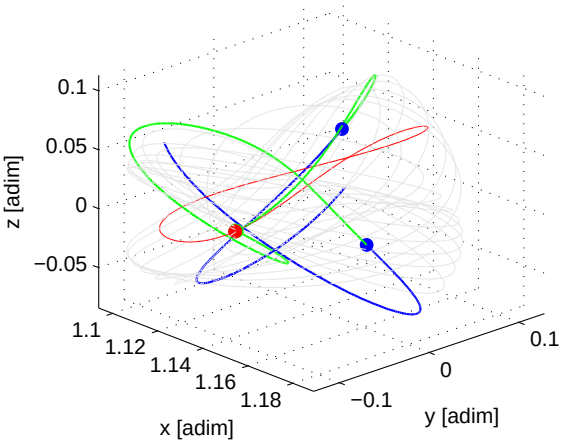

Figure 10: Initial (red) and final (grey) trajectory.

final phases on the quasi-periodic orbit after the transfer are evaluated, see Figure **??**.

For the scenario a feasible transfer solution is highlighted in the plot. Two transfer option are chosen from Figure **??**, the first one series 15 and the second one from series 16. The manoeuvre phase tuples are $\{3.538, 4.865\}$, $\{3.519, 1.2\}$, and $\{xxx, xxx\}$. The time when the manoeuvres are executed is for both solution $t_i = 2.799$. Both spacecraft are transferred at the same time, but the time they reach the final orbit is $t_f^1 = 2.70$ and $t_f^2 = 1.73$ for the second spacecraft. The resulting phase difference of the spacecraft on its new orbit is $\Delta\alpha = 0.019$ and the desired $\Delta\beta = 3.665$. Figure 10 show the path the spacecraft is originally following. The two transfer arcs to the quasi-periodic orbits are highlighted in green, and the final trajectories in blue.

The scenario is visualised in the $\{\alpha, \beta\}$-phase plane. This plot contains various information about the trajectories before and after the transfer. The transfer phase itself is indicated as a line indicating the changes caused by the manoeuvres. The slope of the quasi-periodic orbit in this plot depends on the two system frequencies. The periodic orbit is represented as a line with a second phase angle of $\beta = 0$.

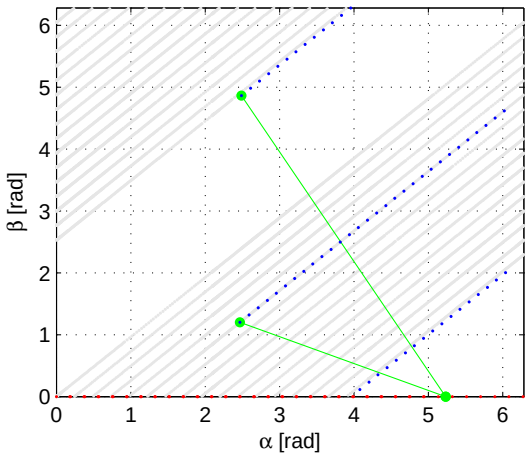

Figure 11: Spacecraft distribution scenario visualised in the $\{\alpha, \beta\}$-phase plane.

V.II Spacecraft phase synchronisation

In the second case, two spacecraft on the same orbit but at different phases (equivalent to true anomalies in keplerian motion) rendezvous by either one or both of the satellites entering transfer trajectories which bring them back to their initial orbit at the same phases, therefore at the same times and locations. This phase synchronization is studied in the following. For a gateway traffic management it is important to reconfigure spacecraft in such a way that they rendezvous in orbit for docking activities. In past studies, phasing manoeuvres are used to fulfil mission requirements, such as for the implementation of eclipse avoidance strategies as quasi-periodic Lissajous suffer of longer eclipse periods compared to halo orbits. In contrast to the amplitude changes of the torus, phases changes maintain the geometric properties as initial and final orbit are identical. They only change the position of an orbiting spacecraft along its trajectory. With respect to the torus theory this implies that the orbit before and after a successful transfer is described by the same quasi-periodic parametric set u.

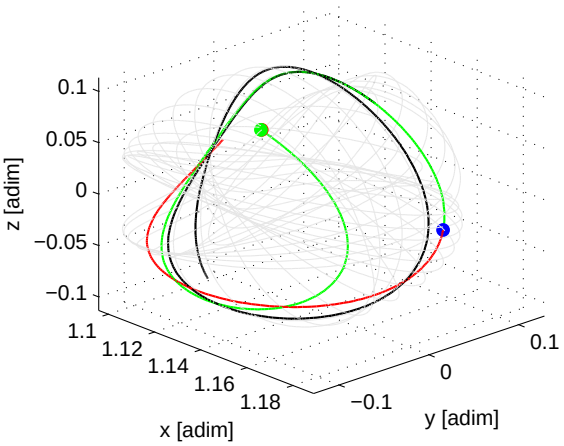

Figure 12: Spacecraft trajectories for second scenario.

A scenario with two spacecraft flying rendezvous manoeuvres on the same quasi-periodic orbit are studied. A pair of spacecraft is inserted onto $\{0, 0\}$ and $\{2.465, 3.680\}$. The objective is that both spacecraft meet at a time t. To provide a parametric analysis on phase changes along a quasi-periodic trajectory, the manifold connections are evaluated. Both spacecraft follow their nominal path until $t = 1.93$ dimensionless units, as seen in Figure 12. The second spacecraft (grey) travelling with an initial phase of $\{0, 0\}$ conducts a manoeuvre. The other spacecraft continues on its nominal path (black). The location of the manoeuvre is highlighted as a green dot, whereas the rendezvous point is indicated in blue. The manoeuvre introduces a phase change of $\Delta\alpha = 2.465$ and $\Delta\beta = 3.680$. After a transfer time of about $t = 2$ both spacecraft rendezvous and follow now on with synchronous phases the quasi-periodic orbit.

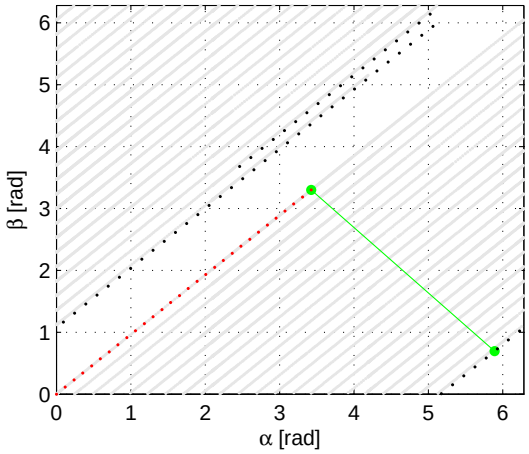

Figure 13: Spacecraft rendezvous scenario visualised in the $\{\alpha, \beta\}$-phase plane.

VI CONCLUSIONS

The exploitation of natural quasi-periodic motion for mission concepts relying on regular rendezvous and docking activities in the lunar vicinity has been proven. The paper proposes a method to calculate transfers between quasi-periodic orbits utilising a parametric representation of the orbit and their manifolds. The numerical methodology to obtain those parametric sets is based on an iterative scheme, which is suitable for the calculation the entire family of quasi-orbits around the far-side Earth-Moon Lagrangian point. The transfer design is based on discretisation methods. The use of the parametric set enables the use of α and β as optimisation variables without numerical integration of the final trajectory. Transfer options are characterised by the transfer times, the phase shifts, and the Δv requirement. A variety of transfers can be calculated with the introduced methods, homo-clinic and hetero-clinic connection as well as transfers to the primary and secondary body. This paper focus on the inner transfer between different quasi-periodic orbits at L_2. Two results of the two scenarios, the spacecraft separation and rendezvous case prove the concept and show the flexibility in introducing regular manoeuvres to phase spacecraft along orbits that remain on a toroidal surface surrounding periodic orbits.

ACKNOWLEDGEMENTS

This work is partially funded through an ESA Networking Partnership Initiative between the University of Strathclyde and the ESA European Space Operations Centre.

REFERENCES

[1] E Canalias. Contributions to Libration Orbit Mission Design using Hyperbolic Invariant Manifolds. 2007.

[2] K Hill and JS Parker. A lunar L2 navigation, communication, and gravity mission. *AIAA/AAS Astrodynamics Specialist Conference*, 2006.

[3] E Kolemen, NJ Kasdin, and P Gurfil. Multiple Poincaré sections method for finding the quasiperiodic orbits of the restricted three body problem. *Celestial Mechanics and Dynamical Astronomy*, 2011.

[4] JM Mondelo and E Barrabés. Numerical parametrisations of libration point trajectories and their invariant manifolds. *AAS/AIAA Astrodynamics Specialists Conference*, 2007.

[5] ZP Olikara and DJ Scheeres. Numerical method for computing quasi-periodic orbits and their stability in the restricted three-body problem. *Conference on Dynamics and Control of Space Systems, Porto Portugal*, 2012.

[6] F Schilder, HM Osinga, and W Vogt. Continuation of Quasiperiodic Invariant Tori. 2004.